Analog quantum chemistry simulation

Javier Argüello-Luengo,[1] Alejandro González-Tudela,[1,2,*] Tao Shi,[1,3] Peter Zoller,[4,1] and J. Ignacio Cirac[1,†]

[1] *Max-Planck-Institut für Quantenoptik, Hans-Kopfermann-Straße 1, D-85748 Garching, Germany*
[2] *Instituto de Física Fundamental IFF-CSIC, Calle Serrano 113b, Madrid 28006, Spain*
[3] *CAS Key Laboratory of Theoretical Physics, Institute of Theoretical Physics, Chinese Academy of Sciences, P.O. Box 2735, Beijing 100190, China*
[4] *Center for Quantum Physics, University of Innsbruck, A-6020 Innsbruck, Austria*

(Dated: July 25, 2018)

Quantum computers hold the promise to provide outstanding computational speed ups in chemical problems, like the determination of the electronic ground state energy of molecules. Here, we demonstrate that the same goal can be achieved with an analog quantum simulator which combines two well-established technologies, namely, ultra-cold atoms in optical lattices and cavity QED. In the proposed simulator, fermionic atoms hopping in an optical potential play the role of electrons, additional optical potentials provide the nuclear attraction, while a single spin excitation over a Mott insulator mediates the electronic Coulomb repulsion. We analyze the impact of discretization and finite size effects of the lattice, and provide the working conditions required for the precise determination of the electronic energy of simple molecules.

Quantum computers are expected to have an enormous impact in several areas of science, as they could tackle problems which are unsolvable with classical devices. Particularly relevant are quantum many-body problems involving several systems interacting with each other according to the rules of Quantum Physics [1]. Among the most timely and significant ones are the so-called quantum chemistry problems, which generally imply obtaining the ground state energy of many electrons interacting with both the nuclei and among themselves through Coulomb interactions. The potential impact in fields like catalysis or drug industry has put the development and implementation of efficient algorithms at the forefront of quantum technology research [2–6].

While full-fledged quantum computers may be built in the future, the next generations will be limited in size and by the presence of errors [7]. An alternative way to address quantum many-body problems is analog quantum simulation [8]. The idea is to use a well-controlled quantum system (the simulator) and engineer its interactions according to the Hamiltonian under investigation. This approach has already yielded results beyond what can be achieved in classical computers [9, 10]. The key feature is that their interactions are either local or short-range, being ideally suited for the existing simulators. On the contrary, analog simulation of quantum chemistry requires engineering long-range (Coulomb) interactions between fermionic particles, and no system has been identified so far fulfilling such requirement. This is why current efforts concentrate in digital simulation [11–13].

In this work we show how to build an analog simulator for quantum chemistry problems by bridging two paradigmatic systems, namely, ultra-cold atoms in optical lattices [14–16] and cavity QED [17–21]. Fermionic atoms trapped in a periodic 3D optical potential play the role of electrons and are subject to additional optical potentials emulating their interaction with the nuclei. The key ingredient of the scheme is to trap another atomic species in the Mott insulator regime, with several internal states such that its spin excitations mediate effective forces between the simulated electrons. We show that even though the interaction is local, one can induce Coulomb-like forces among the fermionic atoms in a scalable manner. While the setup is discrete and finite, we show that precise results can be obtained for simple molecules with moderate lattice sizes. Apart from the standard advantages of analog simulation over quantum computing regarding the required control [8], the present scheme does not rely on a judicious choice of molecular orbitals [22], but directly operates in real space improving convergence to the exact result as the system size increases.

One of the main goals of Quantum Chemistry is to obtain the low energy behavior of N_e electrons and several nuclei when the positions, $\mathbf{r}_n$, of the nuclei are fixed. Using a cubic discretization in real space of $N\times N\times N$ sites, the electronic Hamiltonian to solve contains three terms, $H_{\rm qc} = H_{\rm kin} + H_{\rm nuc} + H_{e-e}$, (using $\hbar = 1$, and dropping the spin index)

$$H_{\rm kin} = -t_F \sum_{\langle \mathbf{i},\mathbf{j}\rangle} f_{\mathbf{i}}^\dagger f_{\mathbf{j}}\,, \tag{1}$$

$$H_{\rm nuc} = -\sum_{n,\mathbf{j}} Z_n V(\|\mathbf{j}-\mathbf{r}_n\|)\, f_{\mathbf{j}}^\dagger f_{\mathbf{j}} \tag{2}$$

$$H_{e-e} = \sum_{\mathbf{i},\mathbf{j}} V(\|\mathbf{i}-\mathbf{j}\|)\, f_{\mathbf{i}}^\dagger f_{\mathbf{i}} f_{\mathbf{j}}^\dagger f_{\mathbf{j}}\,, \tag{3}$$

where $f_{\mathbf{i}}$ are annihilation operators of electrons at site $\mathbf{i}$ fulfilling $\{f_{\mathbf{i}}, f_{\mathbf{j}}^\dagger\} = \delta_{\mathbf{i},\mathbf{j}}$, and $\langle \mathbf{i},\mathbf{j}\rangle$ denote nearest neighbour sites. $H_{\rm kin}$ describes the electrons hopping at a rate t_F, $H_{\rm nuc}$ represents the nuclear attraction when the nuclei are at positions $\mathbf{r}_n$, while H_{e-e} accounts for electron-electron repulsion. In both cases, the attractive/repulsive

* alejandro.gonzalez-tudela@mpq.mpg.de
† ignacio.cirac@mpq.mpg.de

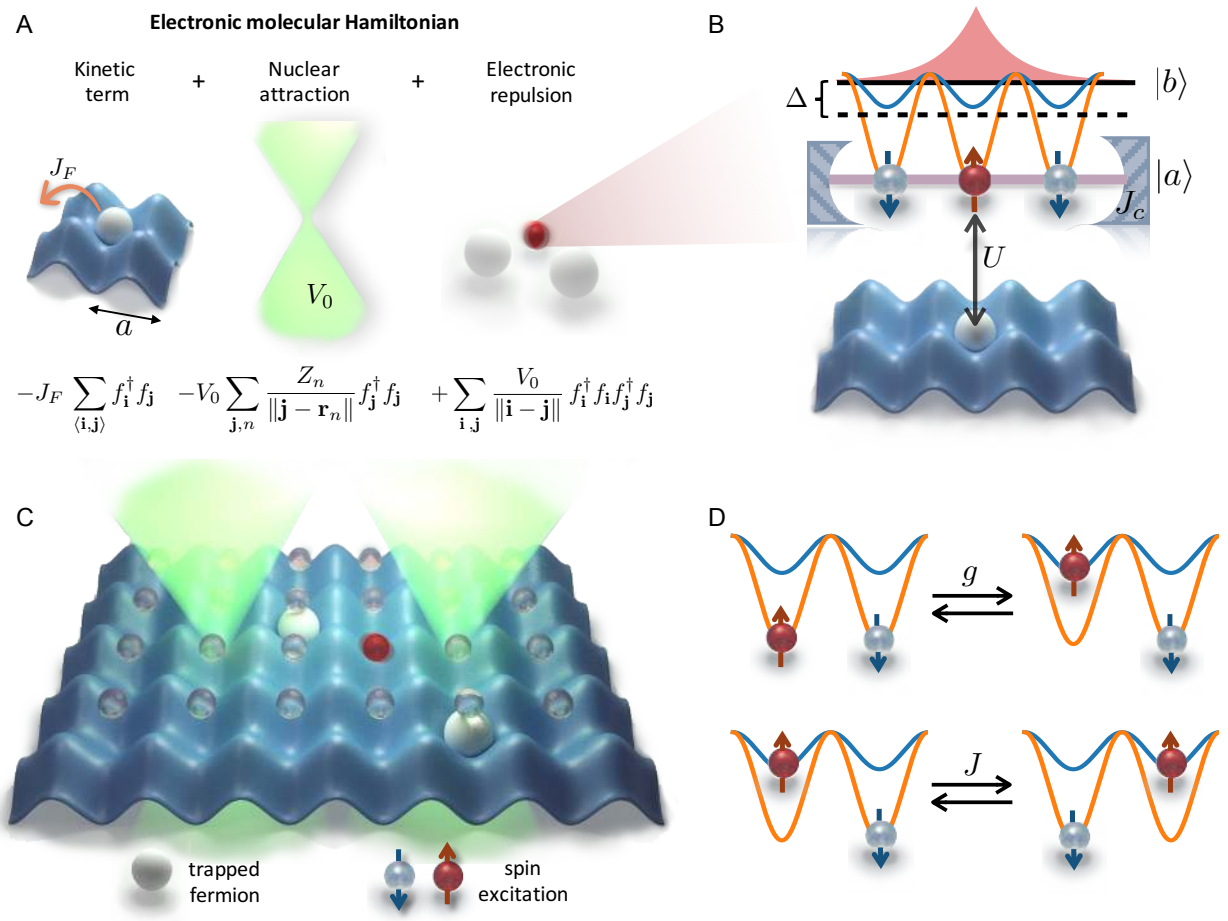

FIG. 1. **Schematic representation of the analog simulator.** (**A**) Fermionic atoms, playing the role of electrons, are trapped in a periodic 3D cubic potential. Their hopping simulates the kinetic energy term of the electrons. Furthermore, they are subject to additional optical potentials which emulate the nuclear interaction. (**B**) Coulomb repulsion among the fermions is mediated by a spin excitation of a Mott insulator with two internal levels. One of the states allows the excitation to propagate through spin exchange interactions with rate J (lower **D**). The other level experiences a strong repulsive interaction with the fermions and interacts with a cavity mode. Both levels are coupled either through a microwave or a two-photon Raman transition (upper **D**). (**C**) Illustration of the complete simulator for the H_2 molecule. While a bidimensional lattice is pictured, the experimental proposal presented here refers to a three-dimensional optical lattice.

potential has the standard Coulomb form, $V(r) = V_0/r$. The connection of the length/energy scales of the discrete Hamiltonian $H_{\rm qc}$ and the continuum one is given by:

$$a_0/a = 2t_F/V_0 \quad \text{and} \quad Ry = V_0^2/(4t_F)\,, \tag{4}$$

where a_0, a and R_y are the Bohr radius, lattice spacing, and Rydberg energy, respectively. Thus, we work in a regime,

$$\text{(a)}\ 1 \ll 2t_F/V_0 \ll N/N_e^{1/3}\,,$$

such that the first inequality prevents discretization effects, and the second guarantees the molecule fits in the volume of the simulator.

Our simulator then requires three ingredients (see Fig. 1A): i) cold spin-polarized fermionic atoms hopping in a 3D optical potential with a tunable tunneling rate, J_F, to play the role of electrons [14, 23]. ii) Additional potentials to emulate the nuclei attraction. Since this is a single-particle Hamiltonian, it can be created through optical Stark-Shifts with an adequate spatial modulation, e.g., using holographic techniques [24, 25]. iii) The most difficult part is to simulate H_{e-e}, since it involves repulsive interactions between the fermions with a $1/r$ dependence. Inspired by how virtual photons mediate Coulomb interactions in QED, we use a spin excitation of another atomic species forming a Mott insulator to mediate the Coulomb forces between fermions (see Fig. 1B). It is composed of N_M^3 atoms trapped in an optical potential with the same spacing as the fermions, and with two additional internal atomic states, a and b, which describe spin excitations. Spin excitations in a state interact repulsively and locally with the fermionic atoms, with strength U,

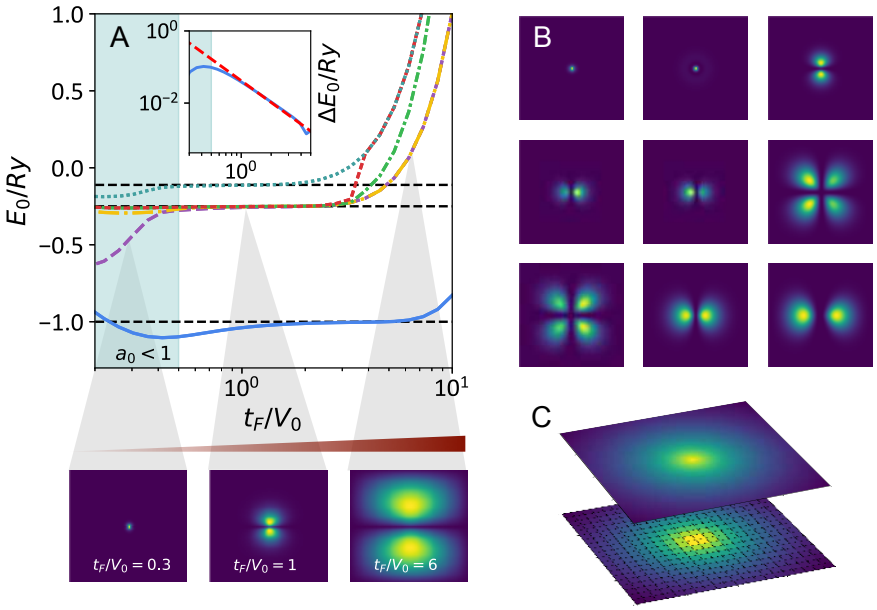

FIG. 2. **Atomic spectrum dependence on the effective Bohr radius.** (**A**) Lower part of the spectrum of the atomic Hamiltonian $H_{\rm qc}$ for a cubic lattice of $N = 100$. Dashed lines indicate the position of the 3 first atomic levels associated to the continuum Hamiltonian. In the colored region, $t_F/V_0 < 0.5$, the Bohr radius is smaller than the lattice spacing and energies are highly affected by the cut-off of the nuclear potential. As the hopping parameter t_F/V_0 increases, the system is effectively zoomed-in, as we show in the panels for the electron density of the second-lowest energy orbital. This includes more lattice sites in the simulation, reducing systematic deviations as $(t_F/V_0)^{-2}$, as we show in the inset for the state associated to the lowest energy state. At higher values of t_F/V_0, solutions suffer from finite-size effects.(**B**) Axial cut in the central positions of the lattice is represented for the first 9 eigenstates of $H_{\rm qc}$ for $t_F/V_0 = 2$, $N = 150$. (**C**) Appropriately choosing the Bohr radius, we show how the same orbital can be obtained with $N = 1000$ (up, $t_F/V_0 = 150$) or $N = 20$ (down, $t_F/V_0 = 3$), where the discretization of the system is more noticeable.

and propagate through the long-range couplings induced by a cavity mode, with rate J_c [17–21]. The b internal state is subject to a different optical potential, such that its itinerant spin excitation propagates through standard nearest-neighbor exchange, at rate J. Furthermore, an external field (Raman laser or a RF field) drives the $a-b$ transition with coupling strength g, and detuning Δ. The complete simulator Hamiltonian after the elimination of the cavity mode reads $H_{\rm sim} = H_{\rm kin} + H_{\rm nuc} + H_M$, with

$$H_M = \Delta \sum_{\mathbf{j}} b^\dagger_{\mathbf{j}} b_{\mathbf{j}} + J \sum_{\langle \mathbf{i},\mathbf{j}\rangle} b^\dagger_{\mathbf{i}} b_{\mathbf{j}} + J_c/N_M^3 \sum_{\mathbf{i},\mathbf{j}} a^\dagger_{\mathbf{i}} a_{\mathbf{j}} + U \sum_{\mathbf{j}} a^\dagger_{\mathbf{j}} a_{\mathbf{j}} f^\dagger_{\mathbf{j}} f_{\mathbf{j}} + g \sum_{\mathbf{j}} \left(a^\dagger_{\mathbf{j}} b_{\mathbf{j}} + b^\dagger_{\mathbf{j}} a_{\mathbf{j}} \right) , \tag{5}$$

being $a_{\mathbf{j}}/b_{\mathbf{j}}$ are annihilation operators for a a/b-spin excitation in site $\mathbf{j}$ [26]. Intuitively, the on-site interaction U localizes the a/b excitations around the fermions, renormalizing their tunneling rates and creating an effective interaction. Mathematically, one can adiabatically eliminate the Mott insulator excitations and derive the effective dynamics for the fermions. The fermionic part of the simulator Hamiltonian $H_{\rm sym} \approx H_{\rm qc}$, with $t_F = J_F(N_e - 1)/N_e$, where the electron-electron potential follows a Yukawa form [27] with a constant energy shift:

$$V(r) \approx C + \frac{V_0}{r/a} e^{-r/L} , \tag{6}$$

where $L/a = \sqrt{J/(U + \Delta + \rho_M J_c - 6J)}$ is the localization length, which can be tuned with Δ, and $V_0 = \frac{g^2}{2\pi J N_e}$ the strength of the potential repulsion. Here $\rho_M = N_e/N_M^3$. This mapping between $H_{\rm sym}$ and $H_{\rm qc}$ holds as long as,

$$\begin{aligned} &\text{(b) } J_c \ll U\,, \quad \text{(c) } J_F, V_0 \ll J_c \cdot \rho_M \,/N_e^{1/2}\,, \\ &\text{(d) } V_0\, N_e^{7/3} \ll J\,(aN/L)^2\,. \end{aligned} \tag{7}$$

Condition (b) enforces that the a excitation localizes symmetrically only around the position of the fermions; (c) guarantees that neither the tunneling of the fermions nor the interaction with the b-excitations spoils the effective interaction; (d) ensures that the Yukawa potential does not depend on the fermionic positions. Furthermore, to obtain a truly Coulomb repulsion, the length L must be larger than the fermionic lattice N, but smaller than the Mott insulator size, that is:

$$\text{(e) } N \ll L/a < N_M.$$

When all (a-e) inequalities are satisfied, the exact solution in the continuum limit is recovered in the limit $N_M > N \to \infty$. Thus, the finite size of the simulator is what ultimately limits the precision of the simulation.

We now benchmark our simulator for moderate system sizes using numerical simulations. In Fig. 2 we solve the Hydrogen problem in a lattice to explore discretization and finite size effects by comparing the energies of the low excited states with that of the continuum. We show that an error of 0.3% with respect to the exact energy can be obtained for systems of $N = 100$. In Fig. 3 we analyze the accuracy for the simplest molecule, H_2. First, we compute exactly the energy of the spin excitation that mediates the fermionic repulsion, as a function of the interfermionic separation (Fig. 3A). We show that it reproduces the $1/r$ behavior over a wide range of values of

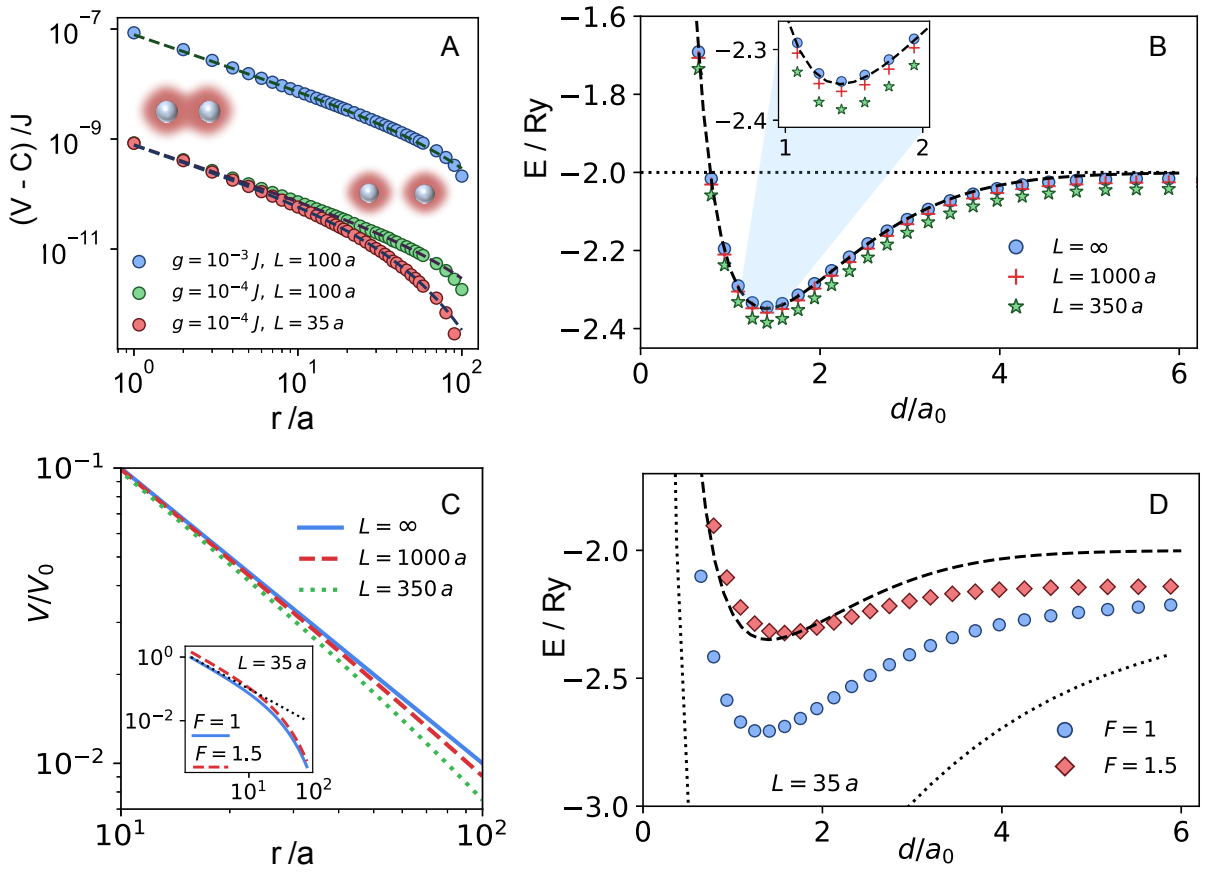

FIG. 3. **Molecular potential and effective interaction mediated by the Mott insulator.** (**A**) Energy of the excited bound state of Hamiltonian (5) with two fixed fermions as a function of their separation, r. We choose $\Delta = 2J$, $N_M = 200$, $J_c = J$, such that (a-e) inequalities are satisfied. The Yukawa potential of Eq. (6) corresponding to each configuration of parameters is plotted with dashed lines. (**B**) We use this effective interaction to calculate the molecular potential associated to an analog simulator of size $N = 75$. For each internuclear separation, we choose t_F/V_0 giving optimal accuracy (see SM for details), ranging from $t_F/V_0 = 4.2$ to $t_F/V_0 = 2.3$ in the dissociation limit (dotted line). Molecular orbitals are included in the projective basis until convergence is observed. For a Coulomb potential (blue dots), the result agrees with an accurate solution in the nonrelativistic regime [28, 29] (dashed line). As L decreases, the exponential decay in the Yukawa potential prevails, underestimating Coulomb repulsion and lowering the molecular potential. (**C**) This underestimation of the repulsive potential is stressed when violating $N \ll L/a$ (see inset). (**D**) Changing the ratio, F between the electronic and nuclear potential, one can explore artificial repulsive interactions that form pseudomolecules in more relaxed experimental conditions. The dotted line represents the limit of zero-repulsion in the absence of a mediating excitation.

g/J and L. In Fig. 3B we compute the molecular potential with $N = 75$ by using a Yukawa electronic potential with different lengths L. We observe excellent qualitative agreement for all L's considered in the figure, and a quantitative matching when $L \gg aN$. Remarkably, even if $L \lesssim aN$, valuable information can still be extracted by adjusting other experimental parameters. In Fig. 3D, we illustrate how one can increase the V_0 of the electron repulsion to compensate the underestimation of the potential at long distances, and obtain a pseudomolecular potential that is qualitatively similar to the one expected with Coulomb interactions.

In conclusion, we demonstrate how to simulate quantum chemistry problems using cold atoms in optical lattices embedded in a cavity. We analyze the required conditions, and perform numerical simulations with the simplest atom and molecule models to assess the accuracy of the simulator, which is ultimately determined by the size of the lattice. Some of the elements and conditions required in this proposal are beyond the state of the art. However, the rapid progress of analog quantum simulation may well lead to the realization of the present ideas in the near future, motivated by its enormous potential impact in the determination of chemical structures, the understanding of reaction mechanisms, or the development of molecular electronics. Furthermore, with judicious changes in the implementation, e.g., different potential geometries, conditions (b-d) may be relaxed. We believe our proposal is a serious alternative to the fault-tolerant quantum computer required to solve the same problems. Furthermore, proof-of-principle versions of our setup, like in one or two dimensions, or with

non Coulomb like potentials, can also be very valuable to benchmark different numerical techniques, develop new theoretical methods, or to reach a deeper understanding of the problems that appear in chemistry. The possibility of analog quantum simulations of quantum chemistry-like problems will strongly stimulate both theoretical and experimental research.

ACKNOWLEDGMENTS

The authors acknowledge the ERC Advanced Grant QENOCOBA under the EU Horizon 2020 program (grant agreement 742102). TS acknowledges the Thousand-Youth-Talent Program of China. PZ was supported by the ERC Synergy Grant UQUAM, and SFB FoQus by the Austrian Science Fundation.

[1] Richard P Feynman, "Simulating Physics with Computers," Int. J. Theor. Phys. **217** (1982).
[2] A. Aspuru-Guzik, A. D. Dutoi, P. J. Love, and M. Head-Gordon, "Simulated Quantum Computation of Molecular Energies," Science **309**, 1704–1707 (2005).
[3] Matthew B Hastings, Dave Wecker, and Matthias Troyer, "Improving quantum algorithms for quantum chemistry," Quantum Inf. Comput. **15**, 1–21 (2015).
[4] Dave Wecker, Bela Bauer, Bryan K. Clark, Matthew B. Hastings, and Matthias Troyer, "Gate-count estimates for performing quantum chemistry on small quantum computers," Phys. Rev. A **90**, 022305 (2014).
[5] Ivan Kassal, James D Whitfield, Alejandro Perdomo-Ortiz, Man-Hong Yung, and Alán Aspuru-Guzik, "Simulating chemistry using quantum computers," Annu. Rev. Phys. Chem **62**, 185–207 (2011).
[6] Markus Reiher, Nathan Wiebe, Krysta M Svore, Dave Wecker, and Matthias Troyer, "Elucidating reaction mechanisms on quantum computers." Proc. Natl. Acad. Sci. U. S. A. **114**, 7555–7560 (2017).
[7] John Preskill, "Quantum Computing in the NISQ era and beyond," (2018), arXiv:1801.00862v2.
[8] J. I. Cirac and P. Zoller, "Goals and opportunities in quantum simulation," Nat. Phys. **8**, 264–266 (2012).
[9] S. Trotzky, Y-A. Chen, A. Flesch, I. P. McCulloch, U. Schollwöck, J. Eisert, and I. Bloch, "Probing the relaxation towards equilibrium in an isolated strongly correlated one-dimensional Bose gas," Nat. Phys. **8**, 325–330 (2012).
[10] Jae-yoon Choi, Sebastian Hild, Johannes Zeiher, Peter Schauß, Antonio Rubio-Abadal, Tarik Yefsah, Vedika Khemani, David A Huse, Immanuel Bloch, and Christian Gross, "Exploring the many-body localization transition in two dimensions." Science **352**, 1547–52 (2016).
[11] P.J.J. O'Malley, R. Babbush, I.D. Kivlichan, J. Romero, J.R. McClean, R. Barends, J. Kelly, P. Roushan, A. Tranter, N. Ding, B. Campbell, Y. Chen, Z. Chen, B. Chiaro, A. Dunsworth, A.G. Fowler, E. Jeffrey, E. Lucero, A. Megrant, J.Y. Mutus, M. Neeley, C. Neill, C. Quintana, D. Sank, A. Vainsencher, J. Wenner, T.C. White, P.V. Coveney, P.J. Love, H. Neven, A. Aspuru-Guzik, and J.M. Martinis, "Scalable Quantum Simulation of Molecular Energies," Phys. Rev. X **6**, 031007 (2016).
[12] Abhinav Kandala, Antonio Mezzacapo, Kristan Temme, Maika Takita, Markus Brink, Jerry M Chow, and Jay M Gambetta, "Hardware-efficient variational quantum eigensolver for small molecules and quantum magnets," Nature **549**, 242–246 (2017).
[13] B. P. Lanyon, J. D. Whitfield, G. G. Gillett, M. E. Goggin, M. P. Almeida, I. Kassal, J. D. Biamonte, M. Mohseni, B. J. Powell, M. Barbieri, A. Aspuru-Guzik, and A. G. White, "Towards quantum chemistry on a quantum computer," Nat. Chem. **2**, 106–111 (2010).
[14] Immanuel Bloch, Jean Dalibard, and Wilhelm Zwerger, "Many-body physics with ultracold gases," Rev. Mod. Phys. **80**, 885–964 (2008).
[15] Kater W. Murch, Kevin L. Moore, Subhadeep Gupta, and Dan M. Stamper-Kurn, "Observation of quantum-measurement backaction with an ultracold atomic gas," Nat. Phys. **4**, 561–564 (2008).
[16] Ludwig Krinner, Michael Stewart, Arturo Pazmino, Joonhyuk Kwon, and Dominik Schneble, "Spontaneous Emission in a Matter-Wave Open Quantum System," (2017), arXiv:1712.07791.
[17] Helmut Ritsch, Peter Domokos, Ferdinand Brennecke, and Tilman Esslinger, "Cold atoms in cavity-generated dynamical optical potentials," Rev. Mod. Phys. **85**, 553–601 (2013).
[18] Sydney Schreppler, Nicolas Spethmann, Nathan Brahms, Thierry Botter, Maryrose Barrios, and Dan M Stamper-Kurn, "Quantum metrology. Optically measuring force near the standard quantum limit." Science **344**, 1486–9 (2014).
[19] Ferdinand Brennecke, Stephan Ritter, Tobias Donner, and Tilman Esslinger, "Cavity optomechanics with a Bose-Einstein condensate." Science **322**, 235–8 (2008).
[20] Ferdinand Brennecke, Tobias Donner, Stephan Ritter, Thomas Bourdel, Michael Köhl, and Tilman Esslinger, "Cavity QED with a BoseEinstein condensate," Nature **450**, 268–271 (2007).
[21] Peter Domokos and Helmut Ritsch, "Collective Cooling and Self-Organization of Atoms in a Cavity," Phys. Rev. Lett. **89**, 253003 (2002).
[22] Attila Szabo and Neil S Ostlund, *Modern quantum chemistry: introduction to advanced electronic structure theory* (Courier Corporation, 2012).
[23] We consider spinless fermions; spin degree of freedom can be included using an extra internal level.
[24] M. R. Sturm, M. Schlosser, R. Walser, and G. Birkl, "Quantum simulators by design: Many-body physics

in reconfigurable arrays of tunnel-coupled traps," Phys. Rev. A **95**, 063625 (2017).
[25] Daniel Barredo, Vincent Lienhard, Sylvain de Léséleuc, Thierry Lahaye, and Antoine Browaeys, "Synthetic three-dimensional atomic structures assembled atom by atom," (2017), arXiv:1712.02727.
[26] We have explicitly written the inverse dependence of the cavity coupling with its volume (N_M^3).
[27] Inés de Vega, Diego Porras, and J Ignacio Cirac, "Matter-Wave Emission in Optical Lattices: Single Particle and Collective Effects," Phys. Rev. Lett. **101**, 260404 (2008).
[28] W Kolost and L Wolniewlczt, "Accurate Adiabatic Treatment of the Ground State of the Hydrogen Molecule New BornOppenheimer potential energy curve and vibrational energies for the electronic ground state of the hydrogen molecule Accurate Adiabatic Treatment of the Ground State of the," J. Chem. Phys. **41**, 2429–3672 (1964).
[29] James S. Sims and Stanley A. Hagstrom, "High precision variational calculations for the Born-Oppenheimer energies of the ground state of the hydrogen molecule," J. Chem. Phys. **124**, 094101 (2006).
[30] Jun John Sakurai and Eugene D Commins, *Modern quantum mechanics,* (Addison-Wesley, 2011).
[31] Weitao Parr, Robert G and Yang, *Density-Functional Theory of Atoms and Molecules* (Oxford University Press, New York, 1989).

SUPPLEMENTARY MATERIAL

Here we provide details about the results and scalings stated in the main text. It is structured as follows: in Section A we describe the main effect of solving the quantum chemistry problem in a discrete lattice system rather than the continuum. We both explain the origin of the inequality (a) and give the details on how to plot Fig. 2 of the main text. In Section B we explain how the effective Coulomb repulsion between fermions emerge in our simulator, and discuss the origin of the inequalities (b-e) in the main text. Finally, in Section C, we discuss both how to optimally choose the simulator parameters to accurately obtain the H_2 molecular potential of Fig. 3, and the numerical method employed to obtain the data in the figure. Finally, in Section D we comment on possible experimental imperfections that may affect the expected behaviour of the simulator.

Appendix A: Discretization and finite size effects in atomic Hamiltonian

In this Section we focus on the effects emerging from both discretization and finite size effects of our simulator. Since we discuss in detail the effect of the fermionic repulsion in sections B and C, here we restrict to the single particle Hamiltonian, that is:

$$H_{\rm kin} + H_{\rm nuc} = -t_F \sum_{\langle \mathbf{i},\mathbf{j}\rangle} f^\dagger_{\mathbf{i}} f_{\mathbf{j}} - \sum_{n,\mathbf{j}} Z_n V(\|\mathbf{j}-\mathbf{r}_n\|)\, f^\dagger_{\mathbf{j}} f_{\mathbf{j}}\,. \tag{A1}$$

The mapping of the typical length/energy scales of the atomic problem, that are the Bohr radius (a_0)/Rydberg energy (R_y) is given in Eq. (4) of the main text. Since this is a quadratic Hamiltonian, we can use exact diagonalization to obtain the lowest part of the spectrum of a single electron and a single nucleus, i.e., an Hydrogen atom. This is what we do in Fig. 2 of the main text for several ratios of t_F/V_0, i.e., for several expected atomic sizes. To avoid the divergence of the nuclear potential, we chose its central point as $(m, m+1/2, m)$, which induces a natural cut-off of the divergence. We also use open boundary conditions in all the figures of the manuscript. To appropriately compare the energies with the continuum limit, we shift the extracted energies by $6t_F$ and finally divide by R_y to express the result in atomic units.

As the Bohr radius increases, we observe that the numerical result approaches the analytical value in the region $1 < a_0/a < N/N_e^{1/3}$, that is, the (a) inequality of the main text for a single electron. The first limit stems from the fact that more than one lattice site is required to properly describe an atomic orbital. The upper-bound of the inequality guarantees that the orbitals fit into the simulator volume to prevent finite-size effects, where we have assumed that the orbital size scales as $N_e^{1/3}$, based on the radial electronic density of alkali atoms. Within this range of parameters, deviations from the analytical value come from the discretization of the lattice. Analytically comparing for Slater wavefunctions, $\psi(r) = 2e^{-r/a_0}/(a_0)^{3/2}$, the integral in the continuum, $\int d\mathbf{r}\psi(\mathbf{r})^2 V(\mathbf{r})$ to the Riemann sum that we are effectively computing, we obtain that the deviation should decrease with the simulator parameter as $(t_F/V_0)^{-2}$, which we numerically confirm for the studied orbitals as shown in the inset of Fig. 2A or the more systematic benchmarking of Fig. S1. We observe that deviations smaller than 0.3% can be obtained for a lattice size $N = 100$ and $t_F/V_0 < 5$.

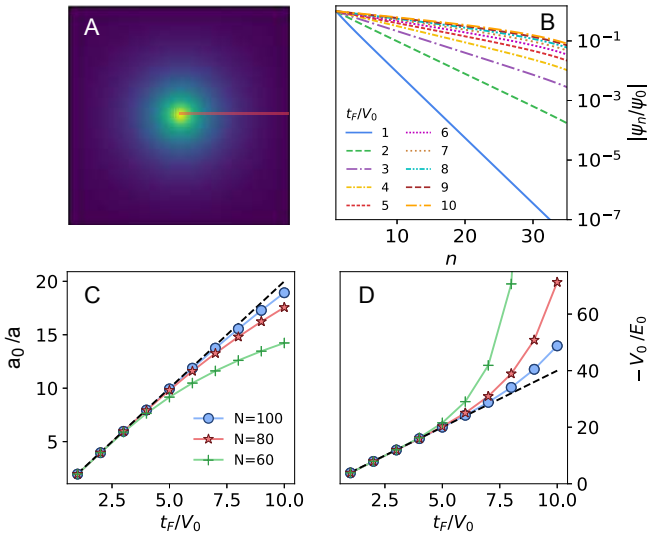

FIG. S1. **Validity of atomic units in finite systems.**(**B**) Radial density of sates associated the ground state of $H_{\rm qc}$ in a cubic lattice with 80 sites per side for different values of t_F/V_0 (in **A** we show an axial cut for $t_F/V_0 = 5$). After normalizing by the central density, log scale reveals the exponential radial decay e^{-r/a_0} characteristic of $1s$ orbitals before finite-size effects appear. A linear fit of the first 30 values provide the decay parameter $1/a_0$. In (**C**), we plot this extracted Bohr radius for different sizes of the lattice and compare it to the scaling in the continuum, $a_0/a = 2t_F/V_0$ (dashed line). The critical Bohr radius at which finite-size effects conspire with the scaling increase linearly with N. This is observation is also appreciated in (**D**) when we compare the energy of this ground state to the dependence in the continuum, $Ry = V_0^2/(4t_F)$ (dashed line).

Appendix B: Effective fermionic repulsion

Obtaining Coloumb repulsion between fermionic atoms is the crucial ingredient of our proposal. In this section, we give full details on how this effective potential emerge, and the conditions (b-e), given in the main text, that need to be satisfied to obtain it.

1. Complete simulator Hamiltonian and analysis procedure

As described in the main text, the complete simulator Hamiltonian is composed by three terms: $H_{\rm sim} = H_{\rm kin}+H_{\rm nuc}+H_M$, namely, the kinetic energy terms given by hopping of the fermionic atoms to nearest neighbour sites with rate J_F, the nuclear potential attraction of $H_{\rm nuc}$, and the H_M, given in Eq. (5) of the main text, which contains both the Mott insulator dynamics and the interaction between the fermionic and Mott insulator atoms.

The way we analyze the problem is to use a Born-Oppenheimer approximation for the fermionic atoms, that is, assuming their timescales are much slower than the Mott insulator atoms dynamics. Like this, we can first solve the Mott-insulator Hamiltonian for each fermionic configuration, and then, self-consistently find both the effect of the Mott-insulator in the fermion dynamics and the conditions under which this Born-Oppenheimer approximation is valid.

Thus, for a given configuration of the fermionic atoms, denoted as, $\{\mathbf{j}\} = \mathbf{j}_1,\ldots,\mathbf{j}_{N_e}$, we make the following decomposition of the Mott-insulator Hamiltonian $H_M(\{\mathbf{j}\}) = H_0 + H_1$, where each term reads:

$$H_0 = U\sum_{\{\mathbf{j}\}} a^\dagger_{\mathbf{j}}a_{\mathbf{j}} + \Delta\sum_{\mathbf{j}} a^\dagger_{\mathbf{j}}a_{\mathbf{j}} + J\sum_{\langle \mathbf{i},\mathbf{j}\rangle} b^\dagger_{\mathbf{i}}b_{\mathbf{j}}\,, \tag{B1}$$

$$H_1 = J_c/N_M^3\sum_{\mathbf{i},\,\mathbf{j}} a^\dagger_{\mathbf{i}}a_{\mathbf{j}} + g\sum_{\mathbf{j}}\left(a^\dagger_{\mathbf{j}}b_{\mathbf{j}} + b^\dagger_{\mathbf{j}}a_{\mathbf{j}}\right)\,, \tag{B2}$$

Notice that $H_M(\{\mathbf{j}\})$ conserves the total number of excitations, $\sum_{\mathbf{j}}\left(a^\dagger_{\mathbf{j}}a_{\mathbf{j}} + b^\dagger_{\mathbf{j}}b_{\mathbf{j}}\right)$. Thus, if we initialize our simulator with a single excitation in Mott-insulator, the dynamics will be restricted to the single-excitation subspace formed by $\mathcal{A}/\mathcal{B} = \{a^\dagger_{\mathbf{j}}/b^\dagger_{\mathbf{j}}\,|0\rangle\}_{\mathbf{j}}$, where $|0\rangle$ is the state with no excitations in the A/B atomic states. The intuition is that the the on-site potential provided by the fermions at positions $\{\mathbf{j}\}$ localizes the Mott-insulator excitations around them forming a bound state. As we will show, the energy of this bound state will depend on the particular fermion configuration, $\{\mathbf{j}\}$, in the same way than the Coulomb potential appearing in chemistry.

To show it, let us first analyze the structure of H_0 in the single-excitation subspace: on the one hand, it contains two degenerate subspaces with $N_e\left[N_M^* \equiv N_M^3 - N_e\right]$ a-states of energy $\Delta + U\,[\Delta]$ that we denote as $\mathcal{A}_U\,[\mathcal{A}\setminus\mathcal{A}_U]$, respectively. On the other hand, the subspace B formed by the b-excitations can be diagonalized if we impose periodic boundary conditions and define the operators $b^\dagger_{\mathbf{k}} = (1/\sqrt{N_M^3})\sum_{\mathbf{j}} e^{-i\mathbf{k}\cdot\mathbf{j}}b^\dagger_{\mathbf{j}}$, which give rise to the energy dispersion: $\omega_{\mathbf{k}} = 2J(\cos(k_x)+\cos(k_y)+\cos(k_z))$.

Now, we treat H_1 as a perturbation of H_0, focusing on the $\mathcal{A}_U$ subspace which is the one coupled directly to the fermions. Since this is a degenerate subspace, we must apply degenerate perturbation theory [30]. This theory assumes that the perturbation, H_1 in our case, breaks the degeneracy in H_0, and starts by choosing an appropriate basis compatible with these new eigenstates. In our case, it is convenient to choose a basis for $\mathcal{A}$ privileging the symmetric combinations of excitations in the $\mathcal{A}_U$ and $\mathcal{A}\setminus\mathcal{A}_U$ subspaces, that can be generally written as:

$$\left|\varphi^{(0)}_X\right\rangle = \frac{1}{\sqrt{\dim(X)}}\sum_{\mathbf{j}\in X} a^\dagger_{\mathbf{j}}\,|0\rangle\,. \tag{B3}$$

where X is the subspace $\mathcal{A}_U$ or $\mathcal{A}\setminus\mathcal{A}_U$ and $\dim(X)$ the dimension of this subspace. In particular, we are interested in the corrections to the symmetric state in $\mathcal{A}_U$, $\left|\varphi^{(0)}_{\mathcal{A}_U}\right\rangle$, which is the one that mediates the correct repulsive potential between the fermions. Thus, we need to calculate:

$$\begin{aligned} E_{s,\mathcal{A}_U} &= E^{(0)}_{s,\mathcal{A}_U} + E^{(1)}_{s,\mathcal{A}_U} + E^{(2)}_{s,\mathcal{A}_U} + \ldots\,, \\ |\varphi_{\mathcal{A}_U}\rangle &= \left|\varphi^{(0)}_{\mathcal{A}_U}\right\rangle + \left|\varphi^{(1)}_{\mathcal{A}_U}\right\rangle + \left|\varphi^{(2)}_{\mathcal{A}_U}\right\rangle + \ldots\,. \end{aligned} \tag{B4}$$

As we will show afterwards $E_{s,\mathcal{A}_U}$ will translate into an effective potential between the fermions, while $\varepsilon = 1 - |\langle\varphi^{(0)}_{\mathcal{A}_U}|\varphi_{\mathcal{A}_U}\rangle|^2$ will be a measure on how much we deviate from the ideal dynamics. Thus, we will impose $\varepsilon \ll 1$ to derive the conditions (b-c) on the main text.

2. Breaking the symmetric state degeneracy with cavity coupling

As prescribed by degenerate perturbation theory, we calculate the perturbed energies/wavefunctions in two steps by separating the contribution of the cavity Hamiltonian $H_{1,c} = J_c/N_M^3\sum_{\mathbf{i},\mathbf{j}} a^\dagger_{\mathbf{i}}a_{\mathbf{j}}$, from the rest of the perturbation $H_{1,g} = H_1 - H_{1,c}$. The cavity Hamiltonian is enough to break the degeneracy of the symmetric states of $\mathcal{A}_U\,[\mathcal{A}\setminus\mathcal{A}_U]$, giving them an extra energy $\rho_M J_c$ $[(1-\rho_M)J_c]$, respectively. Here, we define $\rho_M \equiv N_e/N_M^3$. However, apart from breaking the degeneracy it also couples both symmetric states with strength:

$$\left\langle\varphi^{(0)}_{\mathcal{A}\setminus\mathcal{A}_U}\right| H_{1,c}\left|\varphi^{(0)}_{\mathcal{A}_U}\right\rangle = \sqrt{\rho_M(1-\rho_M)}J_c \approx \sqrt{\rho_M}J_c \tag{B5}$$

where in the last approximation we use $N_e \ll N_M^3$. Thus, in order to keep the mixing between symmetric states small, we must impose $U \gg J_c$, that is inequality (b) of the main text. This guarantees that:

$$E^{(1,c)}_{s,\mathcal{A}_U} \approx \rho_M J_c\,, \tag{B6}$$

and that the first correction to the eigenstate is:

$$\left|\varphi^{(1,c)}_{\mathcal{A}_U}\right\rangle \approx \frac{J_c\sqrt{\rho_M}}{U}\left|\varphi^{(1,c)}_{\mathcal{A}\setminus\mathcal{A}_U}\right\rangle \tag{B7}$$

Notice, that since $\rho_M \ll 1$, the inequality (b) of the main text already guarantees that $J_c\sqrt{\rho_M}/U \ll 1$ and bounds higher order correction in $E^{(c)}_{s,\mathcal{A}_U}$.

3. Non-degenerate perturbation theory with $H_{1,g}$

Once $H_{1,c}$ breaks the degeneracy, we can apply non-degenerate perturbation theory for the rest of the perturbation $H_{1,g}$. To second order, we find:

$$E^{(2,g)}_{s,\mathcal{A}_U} = \frac{g^2}{N_e}\frac{1}{N_M^3}\sum_{\mathbf{k}}\frac{\left|e^{i\mathbf{k}\mathbf{j}_1}+\ldots+e^{i\mathbf{k}\mathbf{j}_{N_e}}\right|^2}{U+\Delta+\rho_M J_c-\omega_{\mathbf{k}}}\,. \tag{B8}$$

In the continuum limit, that is, when $N_M \gg 1$, we can transform the sum into an integral and find:

$$\begin{aligned}\frac{g^2}{N_e}\frac{1}{N_M^3}\sum_{\mathbf{k}}\frac{e^{i\mathbf{k}\mathbf{r}}}{U+\Delta+\rho_M J_c-\omega_{\mathbf{k}}} &\approx \frac{V_0}{2r}e^{-r/L}\,,\\ \frac{g^2}{N_M^3}\sum_{\mathbf{k}}\frac{1}{U+\Delta+\rho_M J_c-\omega_{\mathbf{k}}} &\approx 0.25g^2/J-\frac{aN_eV_0}{2L}\,.\end{aligned} \tag{B9}$$

where $L/a=\sqrt{J/(U+\Delta+\rho_M J_c-6J)}$ is the effective length of the Yukawa-type interaction that appears in $E^{(2)}_{s,\mathcal{A}_U}$. This length can be controlled by the effective detuning between the symmetric state energy $U+\Delta+\rho_M J_c$, and the upper band-edge of $\omega_{\mathbf{k}}$ at $6J$. Notice, that we define $V_0=g^2/(2\pi N_e J)$ as the effective repulsion strength.

Before proceeding to compute the correction to the wavefunction, let us compare the result of the perturbative expansion of the energy with the exact solution of $E_{s,\mathcal{A}_U}$. The latter can be obtained in our problem by solving directly Schrödinger equation, $(H_0+H_1)\left|\Psi_s\right\rangle = E_s\left|\Psi_s\right\rangle$ just imposing that $\left|\Psi_s\right\rangle$ lies in the single-excitation subspace of $\mathcal{A}+\mathcal{B}$. In the conditions of the text, the result is given in the following closed equation:

$$E_{s,\mathcal{A}_U}\approx U+\Delta+\rho_M J_c+\frac{g^2}{N_e}\frac{1}{N_M^3}\sum_{\mathbf{k}}\frac{\left|e^{i\mathbf{k}\mathbf{j}_1}+\ldots+e^{i\mathbf{k}\mathbf{j}_{N_e}}\right|^2}{E_{s,\mathcal{A}_U}-\omega_{\mathbf{k}}}\,. \tag{B10}$$

By comparing both expression, we see that the second order correction introduced by coupling to the b-atomic states must be smaller that $U+\Delta+\rho_M J_c-6J$, which requires the following inequality: $N_e^{7/3}V_0 \ll J(aN/L)^2$. In this estimation, we are using a simplified formula for electron-electron repulsion [31], $V_{e-e}\approx V_0(a/a_0)\left(N_e-1\right)^{2/3}\sum_{\mathbf{j}}\rho^{4/3}(\mathbf{j})$, and approximate an homogeneous electron density, $\rho(\mathbf{j})\approx\rho$, for the optimal situation in which molecular orbitals fully occupy the lattice. This gives the (d) inequality given in the main text.

Finally, let us estimate how much the wavefunction $\left|\varphi^{(0)}_{s,\mathcal{A}_U}\right\rangle$ get perturbed by $H_{1,g}$. To first order:

$$\left|\varphi^{(1,g)}_{s,\mathcal{A}_U}\right\rangle = \sum_{\mathbf{k}}\beta_{\mathbf{k}}\,b^\dagger_{\mathbf{k}}\left|0\right\rangle\,, \tag{B11}$$

whose norm is given by, $\sum_{\mathbf{k}}|\beta_{\mathbf{k}}|^2$, which can be explicitly computed:

$$\sum_{\mathbf{k}}\left|\frac{\langle 0|b_{\mathbf{k}}H_{1,g}|\varphi^{\mathcal{A}_U}_s\rangle}{E^{(0)}_{s\mathcal{A}_U}-\omega_{\mathbf{k}}}\right|^2 = \frac{g^2}{N_e}\frac{1}{N_M^3}\sum_{\mathbf{k}}\frac{\left|e^{i\mathbf{k}\mathbf{j}_1}+\ldots+e^{i\mathbf{k}\mathbf{j}_{N_e}}\right|^2}{\left(U+\Delta+\rho_M J_c-\omega_{\mathbf{k}}\right)^2}\,. \tag{B12}$$

This sum can be calculated taking energy derivatives in (B9), and one obtain the condition, $N_e^{7/3}V_0 \ll aJN^2/L$, which is already guaranteed by imposing the most restrictive condition (d) that we derived by calculating the exact energy of the bound state.

Second order perturbation in $H_{1,g}$ for the wavefunction leads to two type of contributions:

$$\left|\varphi^{(2,g)}_{s,\mathcal{A}_U}\right\rangle = \sum_{s^\perp\mathcal{A}_U}\delta_{s^\perp\mathcal{A}_U}\left|\varphi^{(0)}_{s^\perp\mathcal{A}_U}\right\rangle + \sum_{s^\perp\mathcal{A}\setminus\mathcal{A}_U}\eta_{s^\perp\mathcal{A}_U}\left|\varphi^{(0)}_{s^\perp\mathcal{A}\setminus\mathcal{A}_U}\right\rangle\,, \tag{B13}$$

namely, the ones that the symmetric state to the antisymmetric ones in the $\mathcal{A}_U$ and $\mathcal{A}\setminus\mathcal{A}_U$ subspaces passing by b-states. The norm of the former, $\sum_{s^\perp\mathcal{A}_U}|\delta_{s^\perp\mathcal{A}_U}|^2$, can be approximately upper bounded by:

$$\begin{aligned}&\sum_{s^\perp}\left|\sum_{\mathbf{k}}\frac{\langle\varphi_{s^\perp,\mathcal{A}_U}|H_1 b^\dagger_{\mathbf{k}}|0\rangle\langle 0|b_{\mathbf{k}}H_1|\varphi_{s,\mathcal{A}_U}\rangle}{\left(E^{(0)}_{s,\mathcal{A}_U}-\omega_{\mathbf{k}}\right)\left(E^{(0)}_{s,\mathcal{A}_U}-E^{(0)}_{s^\perp,\mathcal{A}_U}\right)}\right|^2\\ &\qquad<\left(1-1/N_e\right)\frac{V_0^2N_e}{\rho_M^2J_c^2}\,.\end{aligned} \tag{B14}$$

Thus, by imposing it is small we obtain one of the conditions (c) of the main text, i.e., $V_0 \ll \rho_M J_c/\sqrt{N_e}$. The contribution of the antisymmetric state of $\mathcal{A}\setminus\mathcal{A}_U$, that is, $\sum_{s^\perp\mathcal{A}\setminus\mathcal{A}_U}|\eta_{s^\perp\mathcal{A}_U}|^2$ is already small provided that the previous inequalities are satisfied, such that it does not introduce any new condition.

4. Effects on the fermionic dynamics

Once we have calculated the energy of the bound state for each fermionic configuration, $\{\mathbf{j}\}$ now we have to project the fermionic Hamiltonian:

$$H_f = -J_F\sum_{\langle\mathbf{i},\mathbf{j}\rangle}f^\dagger_{\mathbf{i}}f_{\mathbf{j}} + H_{\rm nuc} + U\sum_{\{\mathbf{j}\}}a^\dagger_{\mathbf{j}}a_{\mathbf{j}}f^\dagger_{\mathbf{j}}f_{\mathbf{j}}\,, \tag{B15}$$

into the basis that combines the N_e fermions, with the symmetric spin excitation which mediates the atomic potential, that is:

$$||\mathbf{j}_1\,,\ldots\mathbf{j}_{N_e}\rangle\rangle = \left(f^\dagger_{\mathbf{j}_1}\ldots f^\dagger_{\mathbf{j}_{N_e}}\right)|0\rangle\otimes\left|\varphi_{s,\mathbf{j}_1\ldots\mathbf{j}_{N_e}}\right\rangle\,, \tag{B16}$$

for $\mathbf{j}_1\,,\ldots\mathbf{j}_{N_e}$ any configuration for the position of the N_e fermions. To lowest order one obtains:

$$\tilde{H}_f \approx -t_F\sum_{\langle\mathbf{i},\mathbf{j}\rangle}f^\dagger_{\mathbf{i}}f_{\mathbf{j}} + H_{\rm nuc} + H_{e-e}\,, \tag{B17}$$

where one gets both the electron repulsion Hamiltonian, with a Yukawa potential H_{e-e} and a kinetic energy term

with a reduction of the tunnelling rate, J_F, given by the Frank-Condon overlap:

$$t_F = J_F \langle \varphi_s^{\mathbf{j}_1+1\dots\mathbf{j}_{N_e}} | \varphi_s^{\mathbf{j}_1\dots\mathbf{j}_{N_e}} \rangle \approx J_F \frac{N_e-1}{N_e} \tag{B18}$$

To self-consistently check the validity of the Born-Oppenheimer approach, one must certify that H_f does not efficiently populate states which are not in the basis (B16) we use to project, since H_f can take us out from the symmetric spin excitation, To first order in H_f, the perturbation to our basis states $||\mathbf{j}_1, \dots \mathbf{j}_{N_e}\rangle\rangle$ has the form

$$||\mathbf{j}_1, \dots \mathbf{j}_{N_e}^{(1)}\rangle\rangle = \sum_{s^\perp} \phi^{\mathbf{j}_1\dots\mathbf{j}_{N_e}}_{s^\perp_{\mathbf{j}_1\dots\mathbf{j}_{N_e}}} |\mathbf{j}_1, \dots \mathbf{j}_{N_e}\rangle \otimes \left|\varphi^{s^\perp}_{\mathbf{j}_1\dots\mathbf{j}_{N_e}}\right\rangle , \tag{B19}$$

We can upper bound the perturbation by summing up over the different configurations to arrive to:

$$\sum_{\{\mathbf{j}\}} \sum_{s^\perp} |\phi^{\mathbf{j}_1\dots\mathbf{j}_{N_e}}_{s^\perp_{\mathbf{j}_1\dots\mathbf{j}_{N_e}}}|^2 < \frac{2J_F^2 N_e}{\rho_M^2 J_c^2} , \tag{B20}$$

Imposing that this correction is small, we obtain the other inequality (c) of the main text, that is, $J_F \ll \rho_M J_c/\sqrt{N_e}$.

Finally, there are two additional inequalities related to obtaining a truly Coloumb repulsion rather than a Yukawa. On the one hand, the length of the bound state has to ideally be larger than the fermionic lattice, $L \gg aN$, while being smaller than Mott insulator lattice $L < aN_M$ such that the bound state does not feel the border. Combining both inequalities, we arrive to the condition (e) of the main text.

Appendix C: Obtaining molecular potentials.

In this section, we first give more details on how we choose the simulator parameters to plot the figures of the manuscript, and explain the numerical methods employed for the two-electron wavefunction calculation.

1. Choice of simulator parameters

In Figure 3A we show how the energy of the bound state of the spin excitation as a function on the inter-fermionic separation. We use exact diagonalization of $H_M(\{\mathbf{j}\})$ for two fermions at positions $(m-\lceil d/2\rceil, m, m)$ and $(m+\lfloor d/2\rfloor, m, m)$. Here $\lfloor\cdot\rfloor$ and $\lceil\cdot\rceil$ represent the floor and ceiling functions respectively, and $m = \lfloor N_M/2\rfloor$. To make the figures be placed in a similar scale, we also obtain the energy of the spin excitation bound state when a single fermion is placed at position (m, m, m), and subtract this energy to the two fermions and plot it. In this Figure, we choose the parameters such that the inequalities $(a-e)$ are satisfied and obtain Coulomb repulsion between fermions for $N_M = 200$.

To plot the molecular potential of Fig. 3B, that is, calculate the electronic energy, $E(d)$ as a function of the internuclear distance d, we center the nuclear potential in positions $\mathbf{r}_1 = (m-\lceil d/2\rceil, m+1/2, m)$ and $\mathbf{r}_2 = (m+\lfloor d/2\rfloor, m+1/2, m)$ and obtain the ground state energy using numerical methods that we explain in the next Section. Since two electrons are involved, the extracted energy is now shifted by $12t_F$, and finally written in atomic units. Notice also, that since we use spinless fermions, we have to restrict to the symmetric subspace of the electronic problem so that we can compare the results to those of the H_2 molecule, which is formed for two spins of opposite sign.

As it happens in the atomic case, accuracy increases with the Bohr radius up to a critical value at which finite-size effects are relevant. However, the optimal choice of the Bohr radius now depends on the number of lattice sites that separate the nuclei. To identify this critical Bohr radius at which the finiteness of the lattice $N = 75$ compromises the accuracy, we use the following procedure. First, for a given internuclear separation d/a_0 we solve the electronic structure for nuclear potentials separated a number of lattice sites d/a ranging between 1 and 30, increasing the Bohr radius accordingly, $t_F/V_0 = (d/a)/(2d/a_0)$. The same calculation is repeated for a bigger system size, $N = 100$. Both lattices provide compatible results as long as finite-size effects are not important. The point where both curves deviate corresponds to an approximate optimal t_F/V_0, that provides maximum accuracy for the lattice size considered, e.g., $N = 75$ in our case. In practice, we choose the point at which finite-size energy deviations are one order of magnitude smaller than the discretization error (see Fig. S2). Fitting these values for each internuclear separation d/a, we choose $t_F/V_0 = 4.2 - d/a \cdot 0.065$, i.e., as the nuclei are more separated, the border of the system linearly approaches, needing to reduce the Bohr radius accordingly.

2. Numerical methods to deal with two-electron problem.

Another important difference with respect to the single electron problem is that exact diagonalization strategy is out of reach for our computational resources. To prevent this situation, we artificially reduce the degrees of freedom by projecting the Hamiltonian on a single fermion basis, $\{\phi_i\}_{i=1}^n$. This projected Hamiltonian reads as,

$$H_P = \sum_{i,j,r,s=1}^{n} h_{ijrs} |\phi_i\, \phi_j\rangle \langle \phi_r\, \phi_s| \tag{C1}$$

where $|\phi_i\, \phi_j\rangle$ denotes the product state $|\phi_i\rangle \otimes |\phi_j\rangle$ and $h_{ijrs} = \langle \phi_i\, \phi_j | H_{\text{eff}} | \phi_r\, \phi_s\rangle$.

The success of this strategy depends on how accurately the orbitals in this set can describe the interactions in the Hamiltonian. We then choose a basis composed by

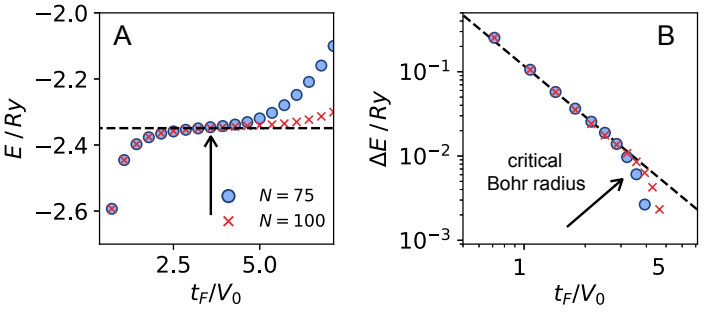

FIG. S2. **Calculation of the critical Bohr radius for H_2.** (**A**) For each internuclear separation d/a_0, we benchmark separations on the lattice d/a ranging from 1 to 25 sites, tuning the Bohr radius accordingly. In the figure, $d = 1.4a_0$, close to the equilibrium distance. Similarly to what happened in the atomic case (see Figure 2A), the calculated potential polynomially approaches the exact solution (dashed line) as the Bohr radius increases, up to the point in which finite size effects appear. To calculate this optimal t_F/V_0, we repeat the calculation for a bigger system, and detect the point where both curves depart. (**B**) To identify this point, we fit the energy of the largest lattice to a universal scaling $m\,(t_F/V_0)^{-2} + n$, (dashed line). For $N = 75$ and a nuclear separation of $1.4a_0$, the critical point (indicated by the arrow) corresponds to $t_F/V_0 \approx 3.5$, providing an expected precision of $10^{-2}Ry$ in the energy of the minimum potential at this given distance.

single-fermion states of H_2^+ calculated with exact diagonalization, together with more orbitals obtained using a Hartree-Fock approximation [22]. Then, starting with the ground state obtained for a single fermion, we iterate the equation,

$$\left(\mathcal{H}_0\left|\phi\right\rangle\right)^{\mathbf{i}} + \sum_{\mathbf{j}} \left(\phi^{\mathbf{j}}\right)^2 V_{12}(\|\mathbf{j}-\mathbf{i}\|)\,\phi^{\mathbf{i}} = \lambda\,\phi^{\mathbf{i}}\,, \tag{C2}$$

until convergence is reached. These orbitals then interact with a mean charge induced by the rest of fermionic atoms in the lattice, while we neglect the exchange interaction.

Once we build an approximated basis, we need to project the Hamiltonian $H_{\rm qc}$ into the basis. The terms associated to the kinetic energy and nuclear interactions are easily projected, as they only depend on single fermionic orbitals, $\langle\phi_i\ \phi_j|\,H_0\,|\phi_r\ \phi_s\rangle = \delta_{js}\,\langle\phi_i|\,H_0\,|\phi_r\rangle + \delta_{ir}\,\langle\phi_j|\,H_0\,|\phi_s\rangle$. The main difficulty comes from calculating terms associated to e-e interactions, $H_{\rm ee}$. At a first glimpse, they involve a sum of N^6 coordinates,

$$\sum_{\mathbf{r}_1,\mathbf{r}_2} V(\mathbf{r}_1-\mathbf{r}_2)\phi_i(\mathbf{r}_1)\phi_r(\mathbf{r}_1)\phi_j(\mathbf{r}_2)\phi_s(\mathbf{r}_2)\,, \tag{C3}$$

where, $V(\mathbf{r}) = V_0/\left\|\mathbf{r}\right\|$ and the lattice imposes a natural cutoff (B9), $V(0) \approx \pi V_0$. In the reciprocal space, this sum simplifies as

$$\langle\phi_i\ \phi_j|\,H_{\rm ee}\,|\phi_r\ \phi_s\rangle = \sum_{\mathbf{k}} \widetilde{V}(\mathbf{k})\cdot\widetilde{(\phi_i\cdot\phi_r)}(\mathbf{k})\cdot\widetilde{(\phi_j\cdot\phi_s)}(-\mathbf{k})\,, \tag{C4}$$

and only N^3 terms are involved, speeding-up the calculation[1]. In principle, this induces periodic boundary conditions in the system, which are undesirable as fermions would interact along the minimum distance measured on the periodic lattice, overestimating e-e interactions. To solve this issue, we double the size of the system before calculating the Fourier transform, and impose null probability of occupying these artificial positions. Fourier Transforms are obtained using a Discrete Fast Fourier Algorithm.

This last calculation is the bottleneck from the computational time perspective and, at the expense of memory, we initially store the FFT for each of the $n(n+1)/2$ product of pairs of molecular orbitals, so that the transformation is not unnecessarily repeated. It is also useful to note that not every term h_{ijrs} needs to be calculated, due to the symmetries of the Hamiltonian. For example, $h_{1123} = h_{1132} = h_{2311} = h_{3211}$. In practice, this reduces the calculated terms from n^4 to $n^2(n^2+3)/4$ independent terms, where n is the number of molecular orbitals in the projected basis. For Figure 3B, we observed that convergence was reached for 15 Hartree-Fock orbitals and 15 low-energy H_2^+ states. This corresponds to $n = 30$, 203175 independent terms, and approximately 8h of total computational time in a 2.20GHz CPU.

The mean charge interaction in the Hartree Fock calculation can also been rewritten as,

$$\sum_{\mathbf{j}} \left(\phi^{\mathbf{j}}\right)^2 V_{12}(\|\mathbf{i}-\mathbf{j}\|)\cdot\phi^{\mathbf{i}} = \langle\phi|\mathcal{F}^{-1}\left(\widetilde{V}(\mathbf{k})\cdot\widetilde{\phi^2}(-\mathbf{k})\right)\rangle\,, \tag{C5}$$

where $\mathcal{F}^{-1}$ denotes the inverse Fourier transform. We should emphasize that this projection on a single-particle basis is just a numerical trick that enables us to numerically benchmark the model, but does not have any impact on the experimental implementation of our proposed analog simulator.

Appendix D: Experimental considerations

Along the manuscript, we derive a set of inequalities (a-e) that our simulator, described by Eq. (5) of the main text, needs to satisfy to reliably simulate the quantum chemistry Hamiltonian. We are, however, aware that there will be other experimental imperfections that may impose extra conditions and that will have to be analyzed in detail to optimize the performance of the simulation. Among the more relevant ones are:

- *Initialization.* The preparation of the initial state has to be carefully designed for the experiment one wants to perform. If one is interested in the

[1] $\widetilde{f}$ denotes the Fourier transform of function f.

ground state properties corresponding to the electronic configuration at a given position of the nuclei, one needs to start in a situation where nuclear potentials are far away from each other and then adiabatically change them to their final position. Furthermore, one should start with parameters in which the Bohr radius is very small, so that the atoms representing the electrons are at fixed positions and then increase their size adiabatically. In any case, the initial state of the spin wave excitation needs to be in a superposition of being at the positions of the electrons. Failing in preparing such state will lead to an unsuccessful simulation.

- *Finite temperature* leads to thermal fluctuations which may spoil the simulation. Thus, these fluctuations will lead to defects in the Mott insulator (see below), an may also influence the internal states of the atoms. The latter, however, can typically be very well controlled in atomic systems as we just need the atoms to be initially in a polarized state, which is reasonably easy to prepare.

- *Dephasing* can be originated by fluctuations in the transitions or due to magnetic fields (as internal levels are being used). This would spoil the potential of the system as a quantum simulator. However, the first effect is small in the case of microwave or Raman transitions, and the second can be controlled in the conditions already used for condensed matter simulations [9, 10].

- *Inexact fermionic filling.* Since fermions play the role of electrons, an inexact number of fermionic atoms hopping in the lattice translates into an erroneous effective charge in the simulated molecule. These errors can be possibly post-selected by measuring the number of electrons after the simulation is performed.

- *Defects in the Mott insulator.* The absence of Mott particles in a given lattice site will locally modify the effective fermion potential. Fermions hopping to this site cannot mediate its repulsive interaction through spin-excitations, perturbing the simulated molecular orbital around this position. Importantly, the defects will not affect the potential far from the fermion such that the final performance of the simulation will scale with the density of defects rather than their number.

- *Spatial inhomogeneities of cavity coupling.* In the simulator Hamiltonian of Eq. (5) of the main text, we have assumed that the a-atoms couple homogeneously to the cavity mode. In general, there might be some inhomogeneities that translates in a Hamiltonian:

$$\frac{J_c}{N_M^3}\sum_{i,j} f_{\mathbf{i},\mathbf{j}} a_{\mathbf{i}}^\dagger a_{\mathbf{j}}\,, \tag{D1}$$

The fluctuations of $f_{\mathbf{i},\mathbf{j}}$ around 1 will induce an extra decoherence timescale, $\Gamma_{c,\mathrm{inh}}$, that must as well be smaller than our simulator parameters.

- *Cavity & atom losses.* Even though the cavity-mediated interactions are mediated by a virtual population of photons, the cavity decay introduces extra decoherence into the system due to the emission of these virtual photons. Moreover, the atomic excited states, also virtually populated, may as well decay to free space introducing losses. Thus, the cooperativity of the cavity QED system must be large to avoid both type of losses.

- *Three-body losses.* Since we have fermions and there can be at most one atom per lattice site, these type of losses should be small.

From these qualitative arguments, we see that most of the possible errors of the simulation are either already under control in current experiments [9, 10] or scale in an intensive way. A quantitative analysis will be presented elsewhere.